PHYSICAL REVIEW D **96,** 102002 (2017)

Performance comparison of multidetector detection statistics in targeted compact binary coalescence gravitational wave searches

K. Haris[*] and Archana Pai[†]

Indian Institute of Science Education and Research Thiruvananthapuram, CET Campus, Trivandrum 695016, India

(Received 19 June 2016; published 8 November 2017)

A global network of advanced interferometric gravitational wave detectors is expected to be on-line soon. Coherent observation of gravitational waves from a distant compact binary coalescence with a network of interferometers located in different continents gives crucial information about the source, such as its location and polarization. In this paper we compare different multidetector network detection statistics for compact binary coalescence searches. In maximum likelihood ratio based detection approaches, the likelihood ratio is optimized to obtain the best model parameters, and the best likelihood ratio value is used as a statistic to make decisions regarding the presence of signals. However, an alternative Bayesian approach involves the marginalization of the likelihood ratio over the parameters and obtains the average likelihood ratio test. We obtain an analytical expression for the Bayesian statistic using the two effective synthetic data streams for targeted searches of nonspinning compact binary systems with an uninformative prior on the parameters. Simulations are carried out to test the validity of the approximation and compare the detection performance with the maximum likelihood ratio and the "hybrid" statistic. We observe that the hybrid statistic gives comparable or better performance with respect to the Bayesian statistic.

DOI: 10.1103/PhysRevD.96.102002

I. INTRODUCTION

A new exciting era of gravitational wave (GW) astronomy has begun with the direct detection of GW signals from binary black hole merger events [1,2] by U.S.-based advanced laser interferometric detectors LIGO-Hanford and LIGO-Livingston [3,4]. The Advanced Virgo detector [5,6] joined the LIGO network and made the first join detection of GW in August 2017 [7]. With upcoming detectors like Japanese cryogenic detector KAGRA [8,9] and U.S.-Indian detector LIGO-India [10], the global network of broadband advanced GW detectors will be able explore the universe in the GW window.

Compact binary coalescences (CBC) with neutron stars and black holes are prime sources of gravitational waves for a ground-based advanced detector network. Based on LIGO's first detections, we expect to see 30 or more binary black hole mergers in the nine-month observation run in 2017–2018 [1]. By 2019, with their design sensitivity, Advanced LIGO detectors could additionally observe ∼40 neutron star binary events and ∼10 neutron star–black hole (NS-BH) events per year [11] along with a hundred or more binary black hole mergers. These numbers would further improve with the new detectors in the global interferometric network.

The classical procedure of detecting GW in interferometric data involves defining a detection statistic, which is a function of data and is compared with a threshold. If all the signal parameters are known, by Neyman-Pearson lemma, any monotonic function of the likelihood ratio $\boldsymbol{\lambda}(\mathbf{x})$—the ratio between probabilities of hypotheses, $\mathcal{H}_S$: the data $\mathbf{x}$ contains signal and $\mathcal{H}_N$: the data $\mathbf{x}$ contains purely noise—is the most powerful detection statistic [12]. Where

$$\boldsymbol{\lambda}(\mathbf{x}) = \frac{\mathbf{P}(\mathbf{x}|\mathcal{H}_S)}{\mathbf{P}(\mathbf{x}|\mathcal{H}_N)}. \tag{1}$$

However, in the GW detection problem, the signal parameters are unknown. Thus, $\mathcal{H}_S$ is a composite hypothesis rather than a simple hypothesis. There are two distinct statistics used to address the composite hypothesis testing problem [12].

(a) T maximum log likelihood ratio (MLR) statistic $\mathcal{L}(x)$ is the maximum of the log of likelihood ratio in the multidimensional signal parameter space $\{\boldsymbol{\Theta}\}$. If $\hat{\boldsymbol{\Theta}}$ is the point in the signal parameter space at which the likelihood ratio in Eq. (1) is maximum, then

$$\mathcal{L}(x) = \ln \boldsymbol{\lambda}(\mathbf{x}, \hat{\boldsymbol{\Theta}}). \tag{2}$$

(b) The Bayesian detection statistic or Bayes factor statistic $\mathcal{B}(x|\Pi)$ is obtained by marginalizing the likelihood ratio over the parameters $\boldsymbol{\Theta}$ with a prior distribution $\mathbf{P}(\boldsymbol{\Theta}|\Pi)$, where the symbol Π denotes all the prior information and assumptions, i.e.,

$$\begin{aligned}\mathcal{B}(\mathbf{x}|I) &= \ln \int_{\boldsymbol{\Theta}} \frac{\mathbf{P}(\mathbf{x}|\boldsymbol{\Theta})}{\mathbf{P}(\mathbf{x}|\mathcal{H}_N\Pi)} \mathbf{P}(\boldsymbol{\Theta}|\Pi)\, d\boldsymbol{\Theta} \\ &= \ln \int_{\boldsymbol{\Theta}} \boldsymbol{\lambda}(\mathbf{x}, \boldsymbol{\Theta}) \mathbf{P}(\boldsymbol{\Theta}|\Pi)\, d\boldsymbol{\Theta}. \end{aligned} \tag{3}$$

[*]haris@iisertvm.ac.in
[†]archana@iisertvm.ac.in

The multidetector MLR approach for CBC signals has been developed in the literature by various groups [13–15]. In this paper we explore the Bayesian approach in the context of multidetector CBC searches.

The paper is divided as follows. In Sec. II, we review the multidetector MLR approach. We show that the multidetector MLR statistic is a Bayesian statistic with an unphysical prior. In Sec. III, we derive an approximate analytic expression for the multidetector Bayesian detection statistic. In Sec. IV, we derive the Bayesian detection statistic tuned for face-on/off binaries and construct a "hybrid" statistic. In Sec. V, we assess the performance of the statistics by comparing the receiver operator characteristic (ROC) curves. Finally in Sec. VI, we summarize and conclude.

II. MLR DETECTION APPROACH FOR CBC SEARCH

The GW signal from a nonspinning compact binary source such as, NS-NS or NS-BH binaries with negligible spin, are characterized by a set of nine parameters $\{m_1, m_2, \mathrm{A}, t_a, \phi_a, \epsilon, \Psi, \theta, \phi\}$, where (m_1, m_2) are the component masses and A is the constant overall amplitude. The phase ϕ_a is the waveform phase at the time of arrival t_a. (ϵ, Ψ) are the binary inclination angle and polarization angle, respectively. (θ, ϕ) characterizes the location of the source on the celestial globe in geocentric coordinates. The time domain GW signal at any m^{th} detector can be written as [15]

$$s_m(t) = \mathrm{F}_{+m} h_+(t) + \mathrm{F}_{\times m} \mathbf{h}_\times(t), \tag{4}$$

where the antenna patterns F_{+m} and $\mathrm{F}_{\times m}$ are functions of source location (θ, ϕ) and the detector Euler angles in geocentric coordinates. A detailed description of coordinates are given in [16].[1] The 3.5 PN restricted nonspinning GW polarizations $h_+(t)$ and $h_\times(t)$ are functions of $\{m_1, m_2, \mathrm{A}, t_a, \phi_a, \epsilon, \Psi\}$. The parameters A, ϵ, Ψ, t_a, and ϕ_a appear in the signal as either a scale or a time/frequency shift. Hence, they are termed as *extrinsic* parameters. The phase evolution of waveform is characterized by the masses $\{m_1, m_2, \}$, which are thus termed as *intrinsic* parameters.

For a global network of I interferometric detectors with uncorrelated noise, the optimum network matched filter SNR square can be expressed as sum of squares of SNRs of individual detectors,[2] i.e.,

$$\boldsymbol{\rho}_s^2 = \sum_{m=1}^{I} \langle \mathbf{s}_m | \mathbf{s}_m \rangle. \tag{5}$$

The corresponding log likelihood ratio for Gaussian noise is given by

$$\ln \boldsymbol{\lambda}(X) = \sum_{m=1}^{I} \langle \mathbf{x}_m | \mathbf{s}_m \rangle - \frac{1}{2} \langle \mathbf{s}_m | \mathbf{s}_m \rangle. \tag{6}$$

The maximization or marginalization of the likelihood ratio over extrinsic parameters $\{A, \phi_a, \cos\epsilon, \Psi\}$ can be done in a straightforward fashion compared to intrinsic parameters. As intrinsic parameters alter the shape of the waveform, maximization/marginalization is a numerical problem. The statistic, which is obtained by either maximizing or marginalizing the likelihood ratio over extrinsic parameters, is then used to search over the remaining intrinsic parameters.

In the following sections we derive and compare MLR and Bayes factor statistics for targeted nonspinning inspiral searches with the multidetector network.

A. Review of coherent multidetector MLR statistic

In this section we review the coherent multidetector network MLR analysis for CBC signal.

The log of network likelihood ratio for I interferometric detectors in the network with uncorrelated Gaussian noises can be written in terms of a pair of synthetic streams as [15],

$$\ln \boldsymbol{\lambda}(X) = \left[\boldsymbol{\rho}_L \langle \mathbf{z}_L | \mathbf{h}_0 e^{i\Phi_L} \rangle - \frac{\boldsymbol{\rho}_L^2}{2} \right] + \left[\boldsymbol{\rho}_R \langle \mathbf{z}_R | \mathbf{h}_0 e^{i\Phi_R} \rangle - \frac{\boldsymbol{\rho}_R^2}{2} \right], \tag{7}$$

Here the overwhitened synthetic streams $\tilde{\tilde{\mathbf{z}}}_{L,R}$ are construed as a linear combination of overwhitened data $\tilde{\tilde{\mathbf{x}}}_m$ from individual detectors as below,

[1] Formally, the parameters (θ, ϕ) are functions of time due to the motion of earth and hence the antenna pattern functions F_{+m} and $\mathrm{F}_{\times m}$ change over time. However, the duration of the binary inspiral signal in the frequency band of the ground-based detectors are very small. Hence, for the case of binary inspiral signals, the antenna pattern functions can be taken as constants over the duration of the signal.

[2] The scalar product of $\mathbf{a}$ and $\mathbf{b}$ is defined as

$$\langle \mathbf{a} | \mathbf{b} \rangle = 4\Re \left[\int_0^\infty \tilde{\tilde{a}}(f) \tilde{b}^*(f) df \right],$$

where $\tilde{\tilde{a}}(f) = \tilde{a}(f)/S_n(f)$ is the double-whitened version of frequency series $\tilde{a}(f)$. The $S_n(f)$ is the one-sided noise power spectral density (PSD) of a detector. In discrete domain,

$$\langle \mathbf{a} | \mathbf{b} \rangle = 4\Re \left[\sum_{j=1}^{N} \tilde{\tilde{a}}_j \tilde{b}_j^* \right],$$

where j is the frequency index.

$$\tilde{\tilde{z}}_L(f) = \sum_{m=1}^{I} \frac{\mathrm{F}_{+m}}{\|\mathbf{F}'_+\|} \tilde{\tilde{x}}_m(f), \qquad \tilde{\tilde{z}}_R(f) = \sum_{m=1}^{I} \frac{\mathrm{F}_{\times m}}{\|\mathbf{F}'_\times\|} \tilde{\tilde{x}}_m(f). \tag{8}$$

$\mathbf{F} = \mathbf{F}_+ + i\mathbf{F}_\times$ is the complex network antenna pattern vector in a dominant polarization frame and $\mathbf{F}' = \mathbf{F}'_+ + i\mathbf{F}'_\times \equiv \{g_m F_m\}$ is the noise weighted version of the same, with the noise weight $g_m = \langle \mathbf{h}_0 | \mathbf{h}_0 \rangle_m$. The dominant polarization frame is the wave frame in which the plus and cross noise weighted antenna pattern vectors are orthogonal to each other in the network space [17]. The dominant polarization frame allows the network log likelihood ratio to be written as a sum of log likelihood ratios of a pair of synthetic detectors. The symbol $\|\cdot\|$ denotes the Euclidean norm of an I-dimensional vector.

The relation between the new set of derived extrinsic parameters $\{\boldsymbol{\rho_L}, \boldsymbol{\rho}_R, \Phi_L, \Phi_R\}$ and physical extrinsic parameters $\{\mathrm{A}, \phi_a, \cos\epsilon, \Psi\}$ is given in Appendix A. The $\boldsymbol{\rho}_{L,R}$ and $\Phi_{L,R}$ act as the SNRs and overall phases of two effective synthetic detectors respectively.

The maximum log likelihood ratio $\mathcal{L}(X)$ maximized over these derived parameters is then a sum of quadratures of the two synthetic streams as given below [14,15],

$$\mathcal{L}(X) = \underbrace{\langle \mathbf{z}_L | \mathbf{h}_0 \rangle^2 + \langle \mathbf{z}_L | \mathbf{h}_{\pi/2} \rangle^2}_{\hat{\rho}_L^2} + \underbrace{\langle \mathbf{z}_R | \mathbf{h}_0 \rangle^2 + \langle \mathbf{z}_R | \mathbf{h}_{\pi/2} \rangle^2}_{\hat{\rho}_R^2}, \tag{9}$$

where $\tilde{\mathbf{h}}_0$ and $\tilde{\mathbf{h}}_{\pi/2} = -i\tilde{\mathbf{h}}_0$ are the two GW phases.

The $\hat{\boldsymbol{\rho}}_{L,R}$ are the maximum likelihood estimates of $\boldsymbol{\rho}_{L,R}$, the SNRs of the synthetic streams. The estimates of $\Phi_{L,R}$ are given by

$$\hat{\Phi}_{L,R} = \arg\left[\sum_{j=1}^{N} \tilde{\tilde{z}}_{L,Rj} \tilde{h}^*_{0j}\right]. \tag{10}$$

B. MLR as viewed in Bayesian framework

In this subsection, we show that the MLR statistic $\mathcal{L}$ can be understood as a $\mathcal{B}$ statistic with an unphysical prior Π_{unph} over the extrinsic parameters.

If we choose the prior on $\{\boldsymbol{\rho}_L, \boldsymbol{\rho}_R, \Phi_L, \Phi_R\}$ as

$$\mathbf{P}(\boldsymbol{\rho}_{L,R}, \Phi_{L,R} | \Pi_{unph}) = C\boldsymbol{\rho_L}\boldsymbol{\rho}_R; \begin{cases} \boldsymbol{\rho}_{L,R} & \in [0, \infty), \\ \Phi_{L,R} & \in [0, 2\pi), \end{cases} \tag{11}$$

the closed-form expression for the Bayesian statistic can be obtained in a straightforward way. The C is a normalization constant. As described earlier, the $\boldsymbol{\rho}_{L,R}$ are the synthetic SNRs and $\Phi_{L,R}$ are the effective phases, and hence take values in the entire range.

Substituting Eqs. (7), (9), (10), and (11) into Eq. (3), we get

$$\begin{aligned} \mathbf{Exp}[\mathcal{B}(X|\Pi_{unph})] &= C \int_0^\infty d\boldsymbol{\rho_L} \int_0^{2\pi} d\Phi_L \boldsymbol{\rho_L} e^{\boldsymbol{\rho_L}\hat{\boldsymbol{\rho}}_L \cos(\Phi_L - \hat{\Phi}_L) - \frac{\boldsymbol{\rho_L}^2}{2}} \\ &\times \int_0^\infty d\boldsymbol{\rho}_R \int_0^{2\pi} d\Phi_R \boldsymbol{\rho}_R e^{\boldsymbol{\rho}_R \hat{\boldsymbol{\rho}}_R \cos(\Phi_R - \hat{\Phi}_R) - \frac{\boldsymbol{\rho}_R^2}{2}}. \end{aligned} \tag{12}$$

By rearranging terms, the integral in Eq. (12) can be converted into a product of four Gaussian integrals, and thus the statistic can be written as

$$\begin{aligned} \mathbf{Exp}[\mathcal{B}(X|\Pi_{unph})] &= 4\pi^2 C e^{\frac{\hat{\boldsymbol{\rho}}_L^2 + \hat{\boldsymbol{\rho}}_R^2}{2}} \\ &= 4\pi^2 C e^{\mathcal{L}(X)/2}, \end{aligned} \tag{13}$$

i.e.,

$$\mathcal{B}(X|\Pi_{unph}) = \frac{\mathcal{L}(X)}{2} + 4\pi^2 C. \tag{14}$$

Eq. (14) clearly indicates that the MLR $\mathcal{L}(X)$ is proportional to the Bayesian statistic $\mathcal{B}(X)$ with a prior Π_{unph}.

To understand the physical meaning of the prior Π_{unph}, we obtain corresponding probability distribution of physical parameters $\{A, \phi_a, \cos\epsilon, \Psi\}$. From Eq. (11), the probability distribution function of physical parameters is given by

$$\begin{aligned} \mathbf{P}(\mathrm{A}, \phi_a, \cos\epsilon, \Psi | \Pi_{unph}) &= C\boldsymbol{\rho_L}\boldsymbol{\rho}_R |J| \\ &= \frac{\mathrm{A}^3 \|\mathbf{F}'_+\|^2 \|\mathbf{F}'_\times\|^2}{4} (1 - \cos^2\epsilon)^3. \end{aligned} \tag{15}$$

Here $|J|$ is the determinant of the Jacobian of transformation from parameter set $\{\boldsymbol{\rho_L}, \Phi_L, \boldsymbol{\rho}_R, \Phi_R\}$ to $\{A, \phi_a, \cos\epsilon, \Psi\}$, i.e.,

$$\begin{aligned} |J| &= \left| \det\left(\frac{\partial\{\boldsymbol{\rho_L}, \Phi_L, \boldsymbol{\rho}_R, \Phi_R\}}{\partial\{\mathrm{A}, \phi_a, \cos\epsilon, \Psi\}} \right) \right| \\ &= \frac{\mathrm{A}^3 \|\mathbf{F}'_+\|^2 \|\mathbf{F}'_\times\|^2 (1 - \cos^2\epsilon)^3}{4\boldsymbol{\rho_L}(\mathrm{A}, \phi_a, \cos\epsilon, \Psi)\boldsymbol{\rho}_R(A, \phi_a, \cos\epsilon, \Psi)}. \end{aligned} \tag{16}$$

(See Appendix A for details.) A close look at Eq. (15) shows that the assumed prior distribution in Eq. (11) is more biased towards the edge-on case compared to the face-on case. However, in reality we expect more binary events from face-on/off systems due to high SNR compared to the edge-on. A similar observation was made in [18] for the case of continuous wave sources, where the connection between the MLR statistic and $\mathcal{B}$ statistic was first obtained in the literature.

III. BAYESIAN STATISTIC FOR A PHYSICAL PRIOR Π_{ph}

In this section we derive a $\mathcal{B}$ statistic for a physical prior. We use an uninformative flat prior for the physical parameters due to lack of any prior information. Making

use of viable approximations, we solve the integral in Eq. (3) to obtain the $\mathcal{B}$ statistic. In the remaining part of the paper the notation $\mathcal{B}$ represents the Bayesian statistic with physical prior Π_{ph} unless and until specified.

A. Physical prior Π_{ph}

The inclination angle ϵ and polarization angle Ψ together form a spherical polar coordinate pair in the "polarization sphere," in which ϵ acts as the polar angle and Ψ acts as the corresponding azimuthal angle. We uniformly sample points from this sphere. We note that $\mathbf{F}_{+,\times}(\Psi) = -\mathbf{F}_{+,\times}(\Psi + \frac{\pi}{2})$, i.e., 2Ψ has $\pi/2$ symmetry in the GW signal. Therefore we choose,

$$\begin{aligned} \mathbf{P}(\cos\epsilon|\Pi_{ph}) &= \frac{1}{2}; \qquad \cos\epsilon \in [-1,1], \\ \mathbf{P}(\Psi|\Pi_{ph}) &= \frac{2}{\pi}; \qquad \Psi \in \left[-\frac{\pi}{4},\frac{\pi}{4}\right]. \end{aligned} \tag{17}$$

The probability distributions of the amplitude A and the initial phase ϕ_a are chosen to be uniform for simplicity, i.e.,

$$\begin{aligned} \mathbf{P}(\phi_a|\Pi_{ph}) &= \frac{1}{2\pi}; \qquad \phi_a \in [0,2\pi], \\ \mathbf{P}(\mathrm{A}|\Pi_{ph}) &= \frac{1}{\mathrm{A}^{\max}}; \qquad \mathrm{A} \in [0,\mathrm{A}^{\max}], \end{aligned} \tag{18}$$

where $\mathrm{A}^{\max}$ is the upper limit for the amplitude.

Thus, the combined prior distribution is

$$\mathbf{P}(\mathrm{A},\phi_a,\cos\epsilon,\Psi|\Pi_{ph}) = \frac{1}{2\pi^2\mathrm{A}^{\max}} \equiv C'. \tag{19}$$

Using $|J|$ in Eq. (A2), we obtain the corresponding distribution for the new extrinsic parameters $\mathbf{P}(\boldsymbol{\rho}_L,\boldsymbol{\rho}_R,\Phi_L,\Phi_R|\Pi_{ph})$ as

$$\mathbf{P}(\boldsymbol{\rho_L},\boldsymbol{\rho_R},\Phi_L,\Phi_R|\Pi_{ph}) = \frac{C'\boldsymbol{\rho_L}\boldsymbol{\rho_R}\left|\frac{\boldsymbol{\rho}_L^2 e^{2i\Phi_L}}{\|\mathbf{F}'_+\|^2} + \frac{\boldsymbol{\rho}_R^2 e^{2i\Phi_R}}{\|\mathbf{F}'_\times\|^2}\right|^{-\frac{3}{2}}}{2\|\mathbf{F}'_+\|^2\|\mathbf{F}'_\times\|^2}. \tag{20}$$

If $\left|\frac{\boldsymbol{\rho}_L^2 e^{2i\Phi_L}}{\|\mathbf{F}'_+\|^2} + \frac{\boldsymbol{\rho}_R^2 e^{2i\Phi_R}}{\|\mathbf{F}'_\times\|^2}\right| = 0$, the probability distribution $\mathbf{P}(\boldsymbol{\rho_L},\boldsymbol{\rho_R},\Phi_L,\Phi_R|\Pi_{ph})$ in Eq. (20) diverges. For that case, the determinant of the Jacobian $|J|$ vanishes, i.e., the transformation between $\{\mathrm{A},\phi_a,\cos\epsilon,\Psi\}$ and $\{\boldsymbol{\rho}_L,\boldsymbol{\rho}_R,\Phi_L,\Phi_R\}$ is invalid. This happens for the face-on/off case, where $\frac{\boldsymbol{\rho}_L}{\|\mathbf{F}'_+\|} = \frac{\boldsymbol{\rho}_R}{\|\mathbf{F}'_\times\|}$ and $\hat{\Phi}_L = \hat{\Phi}_R \pm \frac{\pi}{2}$. In this case, the GW becomes circularly polarized, where Ψ and ϕ_a become degenerate. We exclude this case from the below derivation of $\mathcal{B}$ statistic. We treat face-on/off as a special case and obtain the $\mathcal{B}$ statistic for face-on/off in Sec. IV.

B. Bayesian statistic $\mathcal{B}(X|\Pi_{ph})$

In this subsection, we derive an analytic approximation for the $\mathcal{B}$ statistic. Substitution of Eq. (20) into Eq. (3) gives

$$\begin{aligned} \mathbf{Exp}[\mathcal{B}(X|\Pi_{ph}I)] = \frac{C'}{2\|\mathbf{F}'_+\|^2\|\mathbf{F}'_\times\|^2}\int_0^\infty d\boldsymbol{\rho_L}\int_0^\infty d\boldsymbol{\rho}_R\int_0^{2\pi} d\Phi_L\int_0^{2\pi} d\Phi_R\boldsymbol{\rho_L}\boldsymbol{\rho_R}\left|\frac{\boldsymbol{\rho}_L^2}{\|\mathbf{F}'_+\|^2}e^{2i\Phi_L} + \frac{\boldsymbol{\rho}_R^2}{\|\mathbf{F}'_\times\|^2}e^{2i\Phi_R}\right|^{-\frac{3}{2}} \\ \times \mathrm{Exp}\left[\boldsymbol{\rho_L}\hat{\boldsymbol{\rho}}_L\cos(\Phi_L - \hat{\Phi}_L) - \frac{1}{2}\boldsymbol{\rho}_L^2\right]\mathrm{Exp}\left[\boldsymbol{\rho}_R\hat{\boldsymbol{\rho}}_R\cos(\Phi_R - \hat{\Phi}_R) - \frac{1}{2}\boldsymbol{\rho}_R^2\right]. \end{aligned} \tag{21}$$

In Eq. (21), the numerator contains a product of two separate exponential functions in $\{\boldsymbol{\rho}_L,\Phi_L\}$ and $\{\boldsymbol{\rho}_R,\Phi_R\}$. Compared to these exponential terms, all the remaining terms vary slowly in the parameter range. The product of exponential terms together has a single maximum at the maximum likelihood point $(\hat{\boldsymbol{\rho}}_L,\hat{\boldsymbol{\rho}}_R,\hat{\Phi}_L,\hat{\Phi}_R)$. Assuming the denominator is stationary (slowly varying) around the maximum likelihood point and using Gaussian integral approximation, we can approximate the integral in Eq. (21) as

$$\mathbf{Exp}[\mathcal{B}(X|\Pi_{ph})] \approx \frac{2\pi^2 C' e^{\frac{\hat{\boldsymbol{\rho}}_L^2+\hat{\boldsymbol{\rho}}_R^2}{2}}\left|\frac{\hat{\boldsymbol{\rho}}_L^2}{\|\mathbf{F}'_+\|^2}e^{2i\hat{\Phi}_L} + \frac{\hat{\boldsymbol{\rho}}_R^2}{\|\mathbf{F}'_\times\|^2}e^{2i\hat{\Phi}_R}\right|^{-\frac{3}{2}}}{\|\mathbf{F}'_+\|^2\|\mathbf{F}'_\times\|^2}, \tag{22}$$

or

$$\mathcal{B}(X) \approx \frac{\mathcal{L}(X)}{2} - \frac{3}{2}\ln\left|\frac{\hat{\boldsymbol{\rho}}_L^2 e^{2i\hat{\Phi}_L}}{\|\mathbf{F}'_+\|^2} + \frac{\hat{\boldsymbol{\rho}}_R^2 e^{2i\hat{\Phi}_R}}{\|\mathbf{F}'_\times\|^2}\right| + \text{const.} \tag{23}$$

The detailed derivation of this integral is given in Appendix B.

To summarize, the approximation used in the derivation of $\mathcal{B}(X)$ depends on two conditions:

(a) The denominator of the integrand is not equal to zero around the maximum likelihood point, i.e., the GW signal is not from a face-on/off binary. As mentioned earlier we treat this case in Sec. IV.
(b) Both synthetic stream matched filter SNRs, $\hat{\boldsymbol{\rho}}_L$ and $\hat{\boldsymbol{\rho}}_R$ are reasonably high, or else the corresponding Gaussian integral assumption used in the integration breaks down.

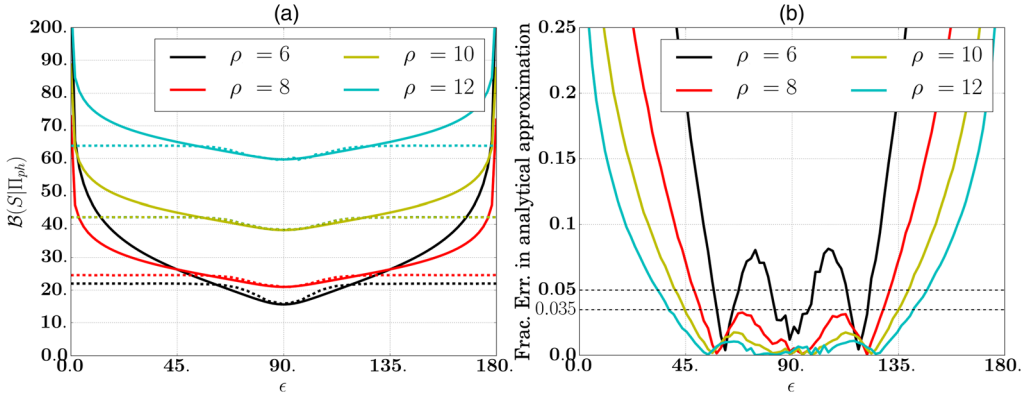

FIG. 1. (a) $\mathcal{B}(X|\Pi_{ph})$ as a function of binary inclination angle ϵ. The dashed curve (solid curve) corresponds to the $\mathcal{B}(X|\Pi_{ph})$ computed numerically (analytically). We assume the data X is purely the signal. (b) Variation of fractional error in analytic approximation with ϵ. The plots are generated for a three detector network LHV. The signal is from (2–10 $M_\odot$) NS-BH system optimally located at $(\theta = 140°, \phi = 100°)$ with an arbitrary polarization angle $\psi = 45°$. We assume "zero-detuning, high power" Advanced LIGO power spectral density [20] for all detectors.

C. $\mathcal{B}$ statistic in $\{\mathrm{A}_L,\mathrm{A}_R\}$ coordinates

In this subsection, we re-express the $\mathcal{B}$ statistic in Eq. (23) in terms of a pair of amplitude coordinates, namely $\mathrm{A}_{L,R} \equiv \mathrm{A}(1 \pm \cos\epsilon)/2$ instead of $\{\boldsymbol{\rho}_L, \boldsymbol{\rho}_R, \Phi_L, \Phi_R\}$.

From Eq. (A1), we can relate $\{\boldsymbol{\rho}_L, \boldsymbol{\rho}_R, \Phi_L, \Phi_R\}$ to $\{\mathrm{A}_L,\mathrm{A}_R\}$ as,

$$|\|\mathbf{F}'_\times\|^2\boldsymbol{\rho}_L^2 e^{2i\Phi_L} + \|\mathbf{F}'_+\|^2\boldsymbol{\rho}_R^2 e^{2i\Phi_R}| \equiv \|\mathbf{F}'_+\|^2\|\mathbf{F}'_\times\|^2\mathrm{A}_L\mathrm{A}_R. \tag{24}$$

Then by substituting Eq. (24) into Eq. (23), $\mathcal{B}(X|\Pi_{ph})$ can be rewritten as

$$\mathcal{B}(X|\Pi_{ph}) = \frac{\mathcal{L}(X)}{2} - \frac{3}{2}\ln[\hat{\mathrm{A}}_L\hat{\mathrm{A}}_R] + \text{const.} \tag{25}$$

This is an alternative representation of the statistic in terms of $\hat{\mathrm{A}}_{L,R}$. In [19], the authors obtained a closed-form expression for the $\mathcal{B}$ statistic with prior Π_{ph} in the continuous waves search context by Taylor expanding the likelihood ratio about its maximum value. The above equation is similar to Eq. (5.37) of [19], which is obtained for continuous GW source context.

D. Validity of the approximation

As described in the previous subsection, the validity of the analytical approximation crucially depends on two conditions. The first one is that the SNR of the signal should be high, and the second one is that the source should not be face-on/off.

In Fig. 1, we have plotted the variation of $\mathcal{B}(X|\Pi_{ph})$ along the inclination angle ϵ of the source for various network SNRs in the absence of noise. The numerical $\mathcal{B}$ statistic is obtained by Monte Carlo (MC) simulation. We used 10^6 MC points for this simulation.

From Fig. 1(b), we note that for all values of SNR $\boldsymbol{\rho}_s$, the fractional error diverges as the inclination angle ϵ approaches, 0° or 180° (face-on/off). This is expected as $|J|$ is zero at these points.

The fractional error in the analytic approximation reduces as $\boldsymbol{\rho}_s$ increases. For example, at $\epsilon = 45°$, the percentage of fractional errors corresponding to $\boldsymbol{\rho}_s = 12, 10, 8, 6$ are 1.8%, 3.1%, 7%, and 19%, respectively. As the $\boldsymbol{\rho}_s$ increases, for a given fractional error, the validity region of this analytic expression increases. For a percentage fractional error of 5%, validity regions vary as $\epsilon \in (48°, 131°)$, $\epsilon \in (40°, 139°)$, and $\epsilon \in (33°, 147°)$ for $\boldsymbol{\rho}_s = 8$, 10, and 12, respectively.

IV. DETECTION STATISTICS FOR FACE-ON/OFF BINARIES

We recall from previous section that the $\mathcal{B}$ statistic obtained with prior Π_{ph} is invalid for the face-on/off cases. This is because, at face-on/off, the signal becomes purely circularly polarized and thus the polarization angle and initial phase are indistinguishable from each other [21]. At $\epsilon = 0$, π the extrinsic parameters in Eq. (A1) can be reduced to

$$\begin{aligned} \boldsymbol{\rho}_L &= \mathrm{A}\|\mathbf{F}'_+\|, \qquad \boldsymbol{\rho}_R = \mathrm{A}\|\mathbf{F}'_\times\| \\ \Phi_L &= \chi + \phi_a, \qquad \Phi_R = \chi + \phi_a \mp \frac{\pi}{2}, \end{aligned} \tag{26}$$

where $\chi \equiv \Psi + \delta/4$. The angle δ is a function of source location and the multidetector network configuration on Earth. For the detailed description of δ, please refer [15]. The amplitudes $\boldsymbol{\rho}_{L,R}$ are constant times the signal amplitude A and Φ_R is $\pi/2$ out of phase with Φ_L. As described earlier, the polarization angle Ψ and the initial phase ϕ_a are degenerate. Due to this degeneracy, the log likelihood ratio for face-on/off binaries can be expressed in terms of only two effective parameters, $\{\boldsymbol{\rho}, \Phi_L\}$, as [21]

$$\ln\boldsymbol{\lambda}^{0,\pi}(X) = \boldsymbol{\rho}\langle\mathbf{z}^{0,\pi}|\mathbf{h}_0 e^{i\Phi_L}\rangle - \frac{1}{2}\boldsymbol{\rho}^2, \tag{27}$$

with $\boldsymbol{\rho} \equiv \mathrm{A}\|\mathbf{F}'\|$ and

$$\tilde{\tilde{z}}^{0}(f) \equiv \sum_{m=1}^{I} \frac{\mathrm{F}_m}{\|\mathbf{F}'\|} \tilde{\tilde{x}}_m(f), \qquad \tilde{\tilde{z}}^{\pi}(f) \equiv \sum_{m=1}^{I} \frac{\mathrm{F}^*_m}{\|\mathbf{F}'\|} \tilde{\tilde{x}}_m(f). \tag{28}$$

A. MLR statistic

In [21,22], the maximization of $\ln \boldsymbol{\lambda}^{0,\pi}(X)$ over $\boldsymbol{\rho}$ and Φ_L is obtained. The MLR is given by,

$$\mathcal{L}^{0,\pi}(X) = \langle \mathbf{z}^{0,\pi} | \mathbf{h}_0 \rangle^2 + \langle \mathbf{z}^{0,\pi} | \mathbf{h}_{\pi/2} \rangle^2, \tag{29}$$

with

$$\hat{\boldsymbol{\rho}} = 4 \left| \sum_{j=1}^{N} \tilde{\tilde{z}}^{0,\pi}_j \tilde{h}^*_{0j} \right|, \qquad \hat{\Phi}_L = \arg \left[\sum_{j=1}^{N} \tilde{\tilde{z}}^{0,\pi}_j \tilde{h}^*_{0j} \right], \tag{30}$$

as the maximum likelihood estimates of $\boldsymbol{\rho}$ and Φ_L.

In contrast with the two-stream generic MLR statistic $\mathcal{L}(X)$, the MLR statistics tuned for face-on/face-off systems $\mathcal{L}^{0,\pi}(X)$ are single stream statistics and reduces the false alarm rate. In [21], the authors show that either $\mathcal{L}^{0}(X)$ or $\mathcal{L}^{\pi}(X)$ capture more than 98% of network matched filter SNR for a wide range of binary inclination angles and polarization angles. Because of the above two properties, a new hybrid statistic, $\mathcal{L}^{mx}(X)$, was proposed as the maximum of $\mathcal{L}^{0}(X)$ and $\mathcal{L}^{\pi}(X)$. The simulations show that the hybrid statistic gives better performance for a wide range of binary inclinations and polarizations [21]. In [22], the authors used a face on/off tuned MLR statistic (single stream) for the GW follow-up search of short gamma ray bursts (GRBs) of InterPlanetary Network (IPN) triggers, which are expected to have small opening angles.

B. Bayesian statistic

In this subsection, we marginalize the likelihood ratio tuned for face-on/off binaries over $\boldsymbol{\rho}$ and Φ_L with the physical prior Π_{ph} discussed in Sec. III A. For face-on/off binaries, the physical prior Π_{ph} in Eq. (18) reduces to

$$\mathbf{P}(\boldsymbol{\rho}, \Phi_L | \Pi_{ph}) = \frac{1}{2\pi \boldsymbol{\rho}^{\max}}, \tag{31}$$

with $\boldsymbol{\rho}^{\max} \equiv \mathbf{A}^{\max}\|\mathbf{F}'\|$. Using Eq. (3), Eq. (27), and Eq. (30), the Bayesian statistic for face-on/off binaries can be written as

$$\begin{aligned} &\mathbf{Exp}[\mathcal{B}^{0,\pi}(X)] \\ &= \int_0^{2\pi} d\Phi_L \int_0^{\boldsymbol{\rho}^{\max}} d\boldsymbol{\rho} \frac{\mathrm{Exp}[\boldsymbol{\rho}\hat{\boldsymbol{\rho}} \cos(\Phi_L - \hat{\Phi}_L) - \frac{1}{2}\boldsymbol{\rho}2]}{2\pi \boldsymbol{\rho}^{\max}} \\ &\approx \frac{1}{\sqrt{2\pi}\boldsymbol{\rho}^{\max}} \int_0^{2\pi} d\Phi_L \mathrm{Exp}\left[\frac{1}{2} \hat{\boldsymbol{\rho}}^2 \cos^2(\Phi_L - \hat{\Phi}_L) \right], \end{aligned} \tag{32}$$

provided $\hat{\boldsymbol{\rho}} \cos(\Phi_L - \hat{\Phi}_L)$ is not close to zero. This condition is reasonable and is satisfied for signals with high SNR, since the integrand will be significant only in a small window of Φ_L around $\hat{\Phi}_L$.

We can approximate $\cos(\Phi_L - \hat{\Phi}_L)$ by $1 - \frac{(\Phi_L - \hat{\Phi}_L)^2}{2}$ and approximate the Φ_L integral by a Gaussian integral. Thus, $\mathcal{B}^{0,\pi}$ can be approximated as

$$\mathbf{Exp}[\mathcal{B}^{0,\pi}(X)] \approx \frac{\sqrt{2}\mathrm{Exp}[\frac{\hat{\boldsymbol{\rho}}^2}{2}]}{\hat{\boldsymbol{\rho}}\boldsymbol{\rho}^{\max}} \tag{33}$$

and

$$\begin{aligned} \mathcal{B}^{0,\pi}(X) &= \frac{\hat{\boldsymbol{\rho}}^2}{2} - \ln[\hat{\boldsymbol{\rho}}\boldsymbol{\rho}^{\max}/\sqrt{2}], \\ &= \frac{1}{2}\mathcal{L}^{0,\pi}(X) - \ln\left[\sqrt{\mathcal{L}^{0,\pi}(X)} \boldsymbol{\rho}^{\max}/\sqrt{2} \right]. \end{aligned} \tag{34}$$

This implies that the $\mathcal{B}^{0,\pi}$ statistic can be approximated by the MLR statistic $\mathcal{L}^{0,\pi}$ with a small logarithmic correction. In the same spirit of $\mathcal{L}^{mx}(X)$, we can define a hybrid Bayesian statistic $\mathcal{B}^{mx}$ as

$$\mathcal{B}^{mx}(X|\Pi_{ph}) = \max[\mathcal{B}^{0}(X), \mathcal{B}^{\pi}(X)]. \tag{35}$$

V. SIMULATIONS AND DISCUSSION

In this section, we carry out numerical simulations for three detector network LHV with LIGO-Livingston (L), LIGO-Hanford (H) and Virgo (V) as the constituent detectors to test the validity of analytical $\mathcal{B}$ statistics and compare the performance of detection statistics using the ROC curve, which is the plot between false alarm probability (FAP) and detection probability (DP). All the detectors are assumed to have additive Gaussian random noise with the noise power spectral density (PSD) following the zero-detuning high power Advanced LIGO noise curve [20]. The simulations are performed for a (2–10 $M_\odot$) NS-BH nonspinning binary signal with fixed optimum network matched filter SNR $\boldsymbol{\rho}_s = 6$.

In this exercise we have used exactly matching mass templates [i.e., (2–10 $M_\odot$)] to filter the data and construct the detection statistics. However, in real searches, one needs to distribute signal templates in mass parameter space and search for the optimum template point. We understand that a template-based search increases the false alarms. However, this is applicable to all the likelihood based statistics. Therefore, the relative detection efficiency study between the likelihood ratio–based statistics will not be affected significantly by fixing the mass parameters of the templates.

A. Performance comparison for fixed injection

In Fig. 2, we have plotted the ROC curves corresponding to MLR based statistics $\mathcal{L}$ and $\mathcal{L}^{mx}$, and the Bayesian statistics $\mathcal{B}(X|\Pi_{ph})$ and $\mathcal{B}^{mx}(X|\Pi_{ph})$ for fixed signal with SNR $\boldsymbol{\rho}_s = 6$ optimally located at $(\theta = 140°, \phi = 100°)$.

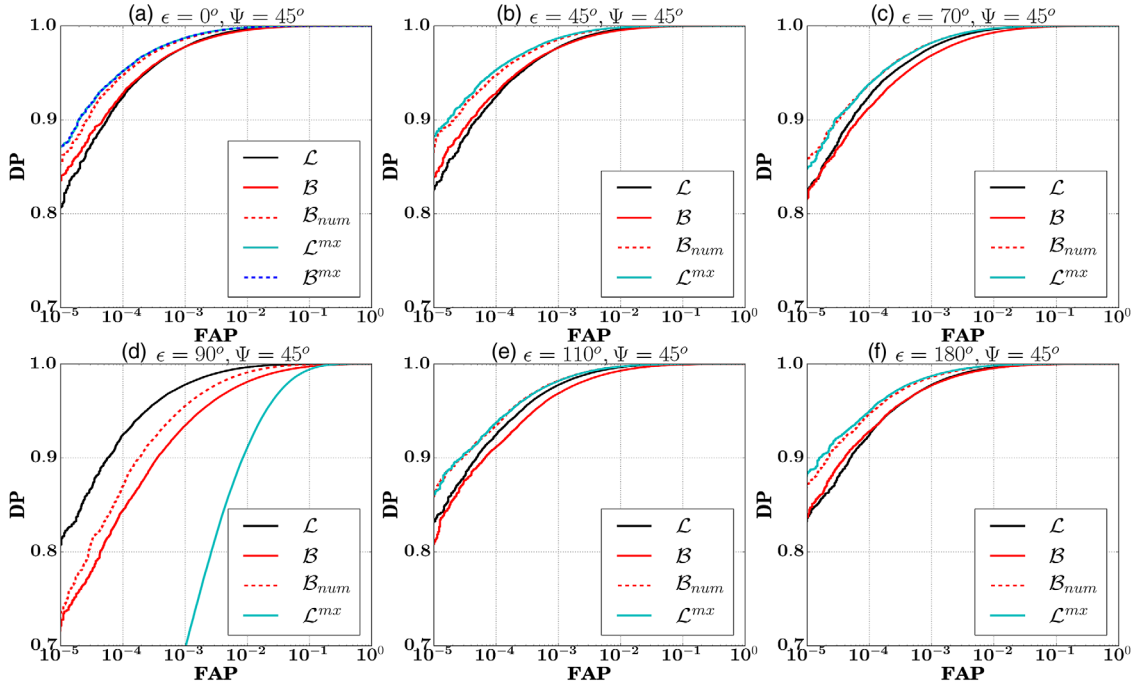

FIG. 2. ROC plots of the statistics corresponding to a network LHV for fixed injections with different values of ϵ. The signal with SNR $\rho_s = 6$ is from (2–10$M\odot$) NS-BH systems optimally located at $(\theta = 140°, \phi = 100°)$ with an arbitrary polarization angle $\psi = 45°$. We assume "zero-detuning high power" Advanced LIGO PSD [20] for all detectors. As one can see in panel (a), the ROC curve of $\mathcal{B}^{mx}$ overlaps with that of $\mathcal{L}^{mx}$. Thus, we omit the ROC curve of $\mathcal{B}^{mx}$ from the remaining panels.

The simulations are performed for six binary inclination angles, namely $\epsilon = 0°$, 45°, 70°, 90°, 110°, 180° and the ROC curves are shown in panels (a), (b), (c), (d), (e), (f) of Fig. 2, respectively. For all cases the binary polarization angle Ψ is arbitrarily fixed to be equal to 45°.

For drawing ROC curves, we have taken 2×10^6 Gaussian noise realizations. For each noise realization, all the statistics are computed with and without signal injection. For each statistic the FAP and DP are computed for different threshold values by counting the number of times each statistic crosses that threshold value when the data contains only the noise as well as when the data contains signal plus noise, respectively.

The ROC curves of the generic MLR statistic $\mathcal{L}$ show small variation with ϵ. On the other hand, the hybrid MLR statistic $\mathcal{L}^{mx}$ shows a preference near the face-on/off region. In [21], we show that the $\mathcal{L}^{mx}$ improves over $\mathcal{L}$ in a wide range of inclination angles except the window 70°–110°.

As we have discussed earlier in Sec. III D, the analytical approximation of the generic Bayesian statistic, $\mathcal{B}(X|\Pi_{ph})$, is reasonably valid only in the neighborhood of $\epsilon = 90°$. We have plotted the ROC curves corresponding to both the numerically calculated Bayesian statistic $\mathcal{B}_{num}$ (dashed red curve) and its analytic approximation $\mathcal{B}$ given in Eq. (23) (solid red curve). The numerical Bayesian statistics are obtained by numerically integrating the likelihood ratio using the Monte Carlo method with 10^6 random draws. For a fixed network optimum matched filter SNR $\rho_s = 6$, the ROC curves corresponding to analytic approximation deviate from $\mathcal{B}_{num}$ for all inclination angles. The detection probability corresponding to the analytical $\mathcal{B}$ always falls below that of $\mathcal{B}_{num}$.

For all inclination angles except $\epsilon = 90°$, the Bayesian statistic (numerical) performs better than the MLR statistic. At edge-on, $\mathcal{L}$ performs better than $\mathcal{B}$. This is expected, as the $\mathcal{L}$ statistic is a Bayesian statistic obtained with an unphysical prior, which is more biased towards edge-on case as described in Sec. II B [see Eq. (14)]. On the other hand, the $\mathcal{B}$ statistic is derived for a flat prior on the polarization sphere. Compared to the hybrid MLR statistic, the Bayesian statistic shows improvement only for the edge-on signal.

The performance of the hybrid Bayesian statistic $\mathcal{B}^{mx}$ always matches with that of $\mathcal{L}^{mx}$. This is because, as one can note in Eq. (34), the Bayesian statistic tuned for face-on/off $\mathcal{B}^{0.\pi}$ is equal to $\mathcal{L}^{0.\pi}$ with a very small logarithmic correction. As $\mathcal{B}^{mx}$ is defined as the maximum of $\mathcal{B}^0$ and $\mathcal{B}^\pi$, it is expected that $\mathcal{B}^{mx}$ shows the same behavior as $\mathcal{L}^{mx}$. Further, the ROC curve corresponding to the analytical approximation of $\mathcal{B}^{mx}$ matches very well that of the numerically evaluated $\mathcal{B}^{mx}$ for all cases. Since the ROC curves of $\mathcal{L}^{mx}$ and $\mathcal{B}^{mx}$ overlap very well, in the figures we explicitly plot the ROC curve corresponding to $\mathcal{B}^{mx}$ only for the $\epsilon = 0$.

In summary,

(a) Near face-on/off cases, the hybrid statistics perform better than the generic statistic $\mathcal{L}$ as well as $\mathcal{B}$.
(b) Near the edge-on case, the generic MLR statistic outperforms all other statistics because of the inbuilt unphysical prior, which is skewed towards the edge-on case.

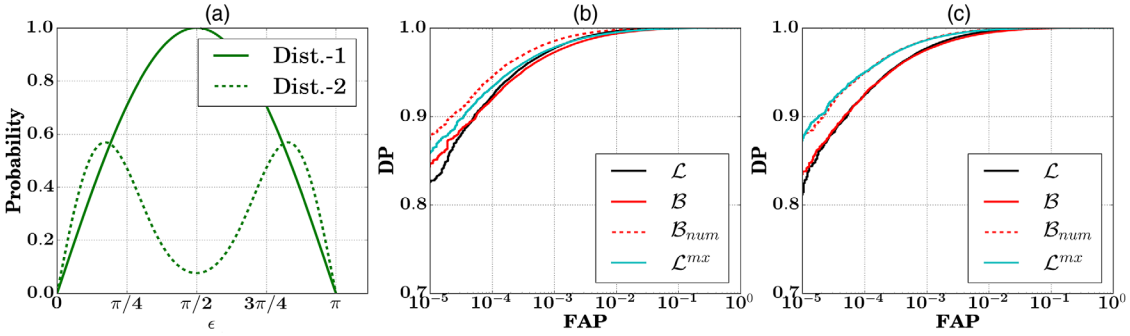

FIG. 3. Panel (a) is the plot of two sampling distributions of ϵ. Panel (b) gives the ROC plots for four different statistics corresponding to a network LHV when the injected signal's inclination angle ϵ is drawn from **Dist-1**, and Panel (c) gives the ROC plots for injections with ϵ drawn from **Dist-2**. In both cases sky location and polarization angles are sampled uniformly. The injections are with SNR $\boldsymbol{\rho}_s = 6$ and are from (2–10$M\odot$) NS-BH systems. We assume "zero-detuning high power" Advanced LIGO PSD [20] for all detectors.

B. Performance comparison for injections sampled from a distribution

In this simulation, the injected binary parameters, inclination angle ϵ, polarization angle Ψ, and source location (θ, ϕ) are sampled from a given distribution. The masses of the binary systems are fixed to be (2–10 $M_\odot$) with the optimum network SNR $\boldsymbol{\rho}_s = 6$. The source location (θ, ϕ) is drawn uniformly from celestial sphere and polarization angle Ψ is sampled uniformly from $[0°, 90°]$. We perform this exercise for two distinct distributions, **Dist-1** and **Dist-2** of inclination angle ϵ.

The **Dist-1** distribution draws $\cos\epsilon$ uniformly from $[-1, 1]$ and is denoted by a green (solid) line in panel (a) of Fig. 3. As seen in the figure, the population of random samples drawn from this distribution contains more edge-on sources than that of face-on.

In **Dist-2**, the ϵ follows the distribution proposed in Eq. (28) of [23] [see green (dashed) line in panel (a) of Fig. 3]. The distribution is given by

$$\mathbf{P}(\epsilon) = 0.076076(1 + 6\cos^2\epsilon + \cos^4\epsilon)^{3/2}\sin\epsilon. \quad (36)$$

Dist-2 is a realistic distribution of ϵ, where the SNR information is folded into the distribution along with the geometric prior. Since we know that the edge-on sources have less SNR than face-on/off sources, we expect to see less edge-on systems than face-on/off ones. As a result, there would be a dip in the curve (dashed line) with respect to the **Dist -1** (solid line).

Figure 3(b) gives the ROC curves corresponding to **Dist-1**, and Fig. 3(c) gives the ROC curves corresponding to **Dist-2**.

For **Dist-1**, the numerical $\mathcal{B}$ statistic outperforms both the generic MLR statistic and hybrid statistics. However, the ROC curve for analytical approximation of the $\mathcal{B}$ statistic does not match with that of the numerically computed $\mathcal{B}$ statistic. For **Dist-2**, the ROC curves of $\mathcal{B}_{num}$ and the hybrid statistics overlap well.

VI. CONCLUSION

The prime motivation behind this work is to develop a Bayesian statistic with a physical prior of the signal parameters as an alternative to the MLR statistic along the lines of [18,19], where the authors develop a Bayesian statistic for the search of continuous gravitational wave signals and compare its performance with the MLR statistic.

In Sec. II B, we have shown that the well-established MLR statistic used for the targeted coherent search of compact binary inspirals is equivalent to a marginalized Bayesian statistic with an unphysical prior over the signal parameters. Further, we obtain an analytic approximation for an alternative Bayesian statistic for the targeted inspiral search with a uniform prior on extrinsic parameters. We also derive a Bayesian statistic tuned for face-on/off binaries and construct a hybrid Bayesian statistic complimentary to the hybrid MLR statistic derived in [21].

We compare the new Bayesian statistics with the coherent MLR-based statistics developed in [13–15] and used for the targeted IPN GRB searches in the LIGO science runs [24,25]. We have demonstrated that the Bayesian statistic shows an improvement of ∼5% in detection probability over the MLR statistic for a false alarm probability of 10^{-5} for the search of near face-on/face-off binary systems. For the sake of completeness, we also compared it with the recently developed hybrid statistic [21]. The hybrid statistic is a phenomenologically developed statistic and is shown to perform better than the MLR statistic for IPN GRB follow-up searches [22]. We observe that the Bayesian statistic shows comparable performance with the hybrid statistic in near face-on/face-off regions.

It is a common belief that MLR statistic is the best possible analytic detection statistic for composite hypothesis testing. However, in this paper we demonstrate that improved closed-form detection statistics are possible by carefully choosing the prior distribution.

Though the coincidence search is established in practice, the benefits of coherent search are well known. The simulations show that the coherent scheme gives ∼10–40% improvement in sensitivity compared to the coincidence approach in binary neutron star searches [14,26,27]. However, due to the higher computational cost of coherent schemes, currently most of the searches are carried out using coincident scheme–based search pipelines. The coherent pipelines are used in the targeted follow-up searches of IPN GRBs [24,25]. The higher computational cost of coherent searches is largely due to the implementation of various χ^2 tests to veto out non-Gaussian glitches from the data. However, by devising efficient hierarchical schemes we can reduce this cost significantly. In hierarchical pipelines we first apply SNR bounds on triggers from individual detectors followed by computation of multidetector coherent detection statistics and less expensive vetoes before computing more accurate expensive vetoes. Thus, in the era of more detectors and high performance computing clusters, the computational cost of coherent schemes is less significant when compared with the advantage in detection efficiency.

ACKNOWLEDGMENTS

The work is supported by MPG-DST Max Planck India Partner Group Grant. The authors availed the 128 cores computing facility established by the MPG-DST Max Planck Partner Group at IISER TVM. We thank the anonymous referee for the critical review and comments.

APPENDIX A: RELATION BETWEEN $\{\mathbf{A}, \boldsymbol{\phi_a}, \boldsymbol{\epsilon}, \boldsymbol{\Psi}\}$ AND $\{\boldsymbol{\rho_L}, \boldsymbol{\rho_R}, \boldsymbol{\Phi_L}, \boldsymbol{\Phi_R}\}$

The derived parameters $\{\boldsymbol{\rho}_L, \boldsymbol{\rho}_R, \Phi_L, \Phi_R\}$ are related to the physical parameters $\{\mathrm{A}, \phi_a, \epsilon, \Psi\}$ as follows:

$$\boldsymbol{\rho_L} e^{i\Phi_L} = \mathrm{A}\|\mathbf{F}'_+\| e^{i\phi_a}\left[\frac{1+\cos^2\epsilon}{2}\cos 2\chi + i\cos\epsilon\sin 2\chi\right],$$
$$\boldsymbol{\rho_R} e^{i\Phi_R} = \mathrm{A}\|\mathbf{F}'_\times\| e^{i\phi_a}\left[\frac{1+\cos^2\epsilon}{2}\sin 2\chi - i\cos\epsilon\cos 2\chi\right]. \tag{A1}$$

The explicit expressions of $\{\boldsymbol{\rho}_L, \boldsymbol{\rho}_R, \Phi_L, \Phi_R\}$ are given in Eq. (B1) of [15]. The determinant of the Jacobian of transformation from $\{\boldsymbol{\rho}_L, \boldsymbol{\rho}_R, \Phi_L, \Phi_R\}$ to $\{\mathrm{A}, \phi_a, \epsilon, \Psi\}$ is given by

$$\begin{aligned}|J| &= \left|\det\left(\frac{\partial\{\boldsymbol{\rho_L}, \Phi_L, \boldsymbol{\rho}_R, \Phi_R\}}{\partial\{\mathrm{A}, \phi_a, \cos\epsilon, \Psi\}}\right)\right| \\ &= \frac{2\|\mathbf{F}'_+\|^2\|\mathbf{F}'_\times\|^2\left|\frac{\boldsymbol{\rho}_L^2 e^{2i\Phi_L}}{\|\mathbf{F}'_+\|^2} + \frac{\boldsymbol{\rho}_R^2 e^{2i\Phi_R}}{\|\mathbf{F}'_\times\|^2}\right|^{3/2}}{\boldsymbol{\rho_L}\boldsymbol{\rho}_R} \\ &= \frac{\mathrm{A}^3\|\mathbf{F}'_+\|^2\|\mathbf{F}'_\times\|^2(1-\cos^2\epsilon)^3}{4\boldsymbol{\rho_L}(\mathrm{A}, \phi_a, \cos\epsilon, \Psi)\boldsymbol{\rho}_R(A, \phi_a, \cos\epsilon, \Psi)}.\end{aligned} \tag{A2}$$

APPENDIX B: APPROXIMATION FOR THE $\mathcal{B}(X|\boldsymbol{\Pi}_{ph})$ INTEGRATION

Equation (21) gives the integral as

$$\mathbf{Exp}[\mathcal{B}(X|\Pi_{ph}I)] = \frac{C'}{2\|\mathbf{F}'_+\|^2\|\mathbf{F}'_\times\|^2}\int_0^\infty d\boldsymbol{\rho_L}\int_0^\infty d\boldsymbol{\rho}_R\int_0^{2\pi} d\Phi_L\int_0^{2\pi} d\Phi_R\boldsymbol{\rho_L}\boldsymbol{\rho}_R\left|\frac{\boldsymbol{\rho}_L^2}{\|\mathbf{F}'_+\|^2}e^{2i\Phi_L} + \frac{\boldsymbol{\rho}_R^2}{\|\mathbf{F}'_\times\|^2}e^{2i\Phi_R}\right|^{-\frac{3}{2}}$$
$$\times \mathrm{Exp}\left[\boldsymbol{\rho_L}\hat{\boldsymbol{\rho}}_L\cos(\Phi_L - \hat{\Phi}_L) - \frac{1}{2}\boldsymbol{\rho}_L^2\right]\mathrm{Exp}\left[\boldsymbol{\rho}_R\hat{\boldsymbol{\rho}}_R\cos(\Phi_R - \hat{\Phi}_R) - \frac{1}{2}\boldsymbol{\rho}_R^2\right]. \tag{B1}$$

The denominator is slowly varying along Φ_L compared to the exponential term in the numerator. If $\boldsymbol{\rho_L}\hat{\boldsymbol{\rho}}_L$ is not small, then $\mathrm{Exp}[\boldsymbol{\rho_L}\hat{\boldsymbol{\rho}}_L\cos(\Phi_L - \hat{\Phi}_L)]$ will be significant only in a very small range of Φ_L around $\hat{\Phi}_L$. Thus, we can approximate $\cos(\Phi_L - \hat{\Phi}_L)$ by $1 - \frac{(\Phi_L - \hat{\Phi}_L)^2}{2}$. By this expansion, the numerator becomes a Gaussian function in Φ_L centered at $\hat{\Phi}_L$. Since the denominator is a slowly varying function of Φ_L compared to the exponential term in the numerator, we can replace Φ_L in the denominator with $\hat{\Phi}_L$ and then approximate the integral by Gaussian integral. Applying a similar argument for Φ_R integration, the $\mathcal{B}$ statistic finally becomes

$$\mathbf{Exp}[\mathcal{B}(X|\Pi_{ph})] \approx \frac{\pi C'}{\|\mathbf{F}'_+\|^2\|\mathbf{F}'_\times\|^2}\int_0^\infty d\boldsymbol{\rho_L}\int_0^\infty d\boldsymbol{\rho}_R\sqrt{\frac{\boldsymbol{\rho_L}\boldsymbol{\rho}_R}{\hat{\boldsymbol{\rho}}_L\hat{\boldsymbol{\rho}}_R}}\frac{\mathrm{Exp}[\boldsymbol{\rho_L}\hat{\boldsymbol{\rho}}_L - \frac{\boldsymbol{\rho}_L^2}{2}]\mathrm{Exp}[\boldsymbol{\rho}_R\hat{\boldsymbol{\rho}}_R - \frac{\boldsymbol{\rho}_R^2}{2}]}{\left|\frac{\boldsymbol{\rho}_L^2}{\|\mathbf{F}'_+\|^2}e^{2i\hat{\Phi}_L} + \frac{\boldsymbol{\rho}_R^2}{\|\mathbf{F}'_\times\|^2}e^{2i\hat{\Phi}_R}\right|^{3/2}}. \tag{B2}$$

Please note this approximation is valid only if the denominator of Eq. (B2) is nonzero.

As one can see in Eq. (B2), the numerator of the integrand can be converted to a product of Gaussian functions in $\boldsymbol{\rho}_L$ and $\boldsymbol{\rho}_R$ centered at $\hat{\boldsymbol{\rho}}_L$ and $\hat{\boldsymbol{\rho}}_R$, respectively. If $\hat{\boldsymbol{\rho}}_L$ and $\hat{\boldsymbol{\rho}}_R$ are large enough, by assuming stationarity for the remaining part of the integrand around $(\hat{\boldsymbol{\rho}}_L, \hat{\boldsymbol{\rho}}_R)$, we can approximate the integrals as

$$\mathbf{Exp}[\mathcal{B}(X|\Pi_{ph})] = \frac{2\pi^2 C' e^{\frac{\hat{\rho}_L^2+\hat{\rho}_R^2}{2}} \left| \frac{\hat{\rho}_L^2}{\|\mathbf{F}'_+\|^2} e^{2i\hat{\Phi}_L} + \frac{\hat{\rho}_R^2}{\|\mathbf{F}'_\times\|^2} e^{2i\hat{\Phi}_R} \right|^{-\frac{3}{2}}}{\|\mathbf{F}'_+\|^2 \|\mathbf{F}'_\times\|^2}. \tag{B3}$$

Now the nonvanishing condition on the denominator of the integrand reduces to

$$\left| \frac{\boldsymbol{\rho}_L^2}{\|\mathbf{F}'_+\|^2} e^{2i\hat{\Phi}_L} + \frac{\boldsymbol{\rho}_R^2}{\|\mathbf{F}'_\times\|^2} e^{2i\hat{\Phi}_R} \right| \neq 0. \tag{B4}$$

In other words, both $\frac{\rho_L}{\|\mathbf{F}'_+\|} - \frac{\rho_R}{\|\mathbf{F}'_\times\|}$ and $\hat{\Phi}_L - \hat{\Phi}_R \pm \frac{\pi}{2}$ are not equal to zero simultaneously. This happens when the signal is either face-on or face-off.

[1] B. P. Abbott, R. Abbott, T. D. Abbott, M. R. Abernathy, F. Acernese, K. Ackley, C. Adams, T. Adams, P. Addesso, R. X. Adhikari *et al.* (LIGO Scientific Collaboration and Virgo Collaboration), Phys. Rev. Lett. **116**, 061102 (2016).

[2] B. P. Abbott *et al.* (Virgo Collaboration and LIGO Scientific Collaboration), Phys. Rev. Lett. **116**, 241103 (2016).

[3] J. Aasi, B. P. Abbott, R. Abbott, T. Abbott, M. R. Abernathy, K. Ackley, C. Adams, T. Adams, P. Addesso *et al.* (The LIGO Scientific Collaboration), Classical Quantum Gravity **32**, 074001 (2015).

[4] G. M. Harry (LIGO Scientific), Classical Quantum Gravity **27**, 084006 (2010).

[5] F. Acernese *et al.* (Virgo Collaboration), Classical Quantum Gravity **32**, 024001 (2015).

[6] T. Accadia *et al.* (Virgo Collaboration) Report No. VIR-0128A-12, 2012.

[7] B. P. Abbott *et al.*, Phys. Rev. Lett. **119**, 141101 (2017).

[8] Y. Aso, Y. Michimura, K. Somiya, M. Ando, O. Miyakawa, T. Sekiguchi, D. Tatsumi, and H. Yamamoto (The KAGRA Collaboration), Phys. Rev. D **88**, 043007 (2013).

[9] K. Somiya, Classical Quantum Gravity **29**, 124007 (2012).

[10] B. Iyer *et al.*, LIGO Document Control Center Report No. LIGO-M1100296-v2, 2011.

[11] J. Abadie, B. P. Abbott, R. Abbott, M. Abernathy, T. Accadia, F. Acernese, C. Adams, R. Adhikari, P. Ajith, B. Allen *et al.*, Classical Quantum Gravity **27**, 173001 (2010).

[12] C. W. Helstrom, *Statistical Theory of Signal Detection* (Pergamon Press, New York, 1960).

[13] A. Pai, S. Dhurandhar, and S. Bose, Phys. Rev. D **64**, 042004 (2001).

[14] I. W. Harry and S. Fairhurst, Phys. Rev. D **83**, 084002 (2011).

[15] K. Haris and A. Pai, Phys. Rev. D **90**, 022003 (2014).

[16] A. Pai, E. Chassande-Mottin, and O. Rabaste, Phys. Rev. D **77**, 062005 (2008).

[17] S. Klimenko, S. Mohanty, M. Rakhmanov, and G. Mitselmakher, Phys. Rev. D **72**, 122002 (2005).

[18] R. Prix and B. Krishnan, Classical Quantum Gravity **26**, 204013 (2009).

[19] J. T. Whelan, R. Prix, C. J. Cutler, and J. L. Willis, Classical Quantum Gravity **31**, 065002 (2014).

[20] D. Shoemaker, LIGO Document Control Center Report No. LIGO-T0900288-v3, 2010.

[21] K. Haris and A. Pai, Phys. Rev. D **93**, 102002 (2016).

[22] A. Williamson, C. Biwer, S. Fairhurst, I. Harry, E. Macdonald, D. Macleod, and V. Predoi, Phys. Rev. D **90**, 122004 (2014).

[23] B. F. Schutz, Classical Quantum Gravity **28**, 125023 (2011).

[24] J. Abadie, B. P. Abbott, R. Abbott, T. D. Abbott, M. Abernathy, T. Accadia, F. Acernese, C. Adams, R. X. Adhikari, C. Affeldt *et al.*, Astrophys. J. **760**, 12 (2012).

[25] J. Aasi, B. P. Abbott, R. Abbott, T. Abbott, M. R. Abernathy, F. Acernese, K. Ackley, C. Adams, T. Adams, P. Addesso *et al.* (LIGO Scientific Collaboration, Virgo Collaboration, and IPN Collaboration), Phys. Rev. Lett. **113**, 011102 (2014).

[26] H. Mukhopadhyay, N. Sago, H. Tagoshi, S. Dhurandhar, H. Takahashi, and N. Kanda, Phys. Rev. D **74**, 083005 (2006).

[27] H. Mukhopadhyay, H. Tagoshi, S. Dhurandhar, and N. Kanda, Phys. Rev. D **80**, 123019 (2009).